IJE TRANSACTIONS B: Applications Vol. 34, No. 05, (May 2021) 1105-1117

International Journal of Engineering

Journal Homepage: www.ije.ir

The Effects of Mathematical Modelling of Magneto-rheological Dampers on Its Control Performance: A Comparative Study Between the Modified Bouc-Wen and the Maxwell Nonlinear Slider Hysteretic Models

R. Karami Mohammadi, H. Ghamari*

School of Civil and Environmental Engineering, KN Toosi University of technology, Tehran, Iran

P A P E R I N F O

Paper history:
Received 18 October 2020
Received in revised form 13 March 2021
Accepted 24 March 2021

Keywords:
Magneto-rheological Damper
Semi-active Control
Maxwell Nonlinear Slider Model
Bouc-Wen Model
Linear Quadratic Regulator Algorithm
Nonlinear Instantaneous Optimal Control

A B S T R A C T

Input voltage of Magneto Rheological (MR) dampers is the only controllable parameter as a semi-active control device. Therefore, voltage selection has an important role in control procedure via MR dampers. In many of semi-active control algorithms, a mathematical modelling method is required for determining the MR damper voltage at each time instant. As a result, applying different mathematical modelling methods can lead to different voltages for the MR damper, which subsequently results in different control performance. In the present research, the effects of mathematical modelling method of an MR damper hysteretic behaviour on its control performance were investigated. The most exact and common Maxwell nonlinear slider and modified Bouc-Wen hysteretic models were employed through a nonlinear comparative numerical study. A building structure was utilized for numerical investigations. A ten-story office building steel structure is excited by seven acceleration time histories. Nonlinear instantaneous optimal control and linear quadratic regulator controllers were utilized as two active-based semi-active algorithms. Results of nonlinear investigations showed an obvious difference between the Maxwell nonlinear slider and the modified Bouc-Wen models from the control performance viewpoint. Outputs show a very slight better performance for the MNS model in reducing the nonlinear responses.

***doi**: 10.5829/ije.2021.34.05b. 04*

NOMENCLATURE

R , Q	Wheighting matrices	J	Performance index
A	open-loop plant matrix	B	Control force locating matrix
M , C , K	Mass, damping, stiffness matrices	$\ddot{x}_g$	Ground acceleration
E_h	Hysteretic energy	ζ , η	Constants of NIOC algorithm
ρ	Constant	P	solution of the Riccati equation
$\{H\}$, $\{\delta\}$	Force-adjustment vectors	u	Control input
$\{z(t)\}$	State vector	k	Optimal gain matrix
x , $\dot{x}$, $\ddot{x}$	Vector of relative displacement, velocity, and acceleration response.	$f_v(t)$, $f_x(t)$	Internal force vectors
y , z	Variables of the modified Bouc-Wen and MNS models	Δt	Lattice time step
$\alpha, c_o, k_o, k_1, c_1, n, A$	Modified Bouc-Wen parameters	c, k, a, b, n, m_o	MNS model parameters
I , O	Identity and zero matrices	Δ , Δ_R	Interstory drift and residual drift

* Corresponding Author Email: hghamari@mail.kntu.ac.ir (H. Ghamari)

Please cite this article as: R. Karami Mohammadi, H. Ghamari. The Effects of Mathematical Modelling of Magneto-rheological Dampers On Its Control Performance; A Comparative Study Between the Modified Bouc-Wen and the Maxwell Nonlinear Slider Hysteretic Models, International Journal of Engineering, Transactions B: Applications Vol. 34, No. 05, (2021) 1105-1117

1. INTRODUCTION

Vibration control of structures intends to preserve the vibration behaviour of a structure within a desired range. Ha [1] used a method for the reduction of rotor blade vibrations and noise. There are several types of motion control for a structure. In a performance viewpoint, there are three control categories: Active, passive, and semi-active manners. Passive control devices generate control force using the local response of the installation location. Characteristics of passive devices are not changeable. Active control devices generate control forces using an external source of electric power based on a pre-defined control algorithm. However, there is a deficiency: the drawback of this category is that, external power supply may disconnect during severe earthquakes. Also, the energy which is applied to the structure by active devices may lead to instability. On the other side, this control type is adaptable. Semi-active control devices produce control forces utilizing the local response of the installation location of device. Nevertheless, a semi-active device can change its characteristics during the excitation using a relatively small power supply e.g., a few batteries. Therefore, this system enjoys the positive features of both active and passive vibration control systems, namely, adaptability and stability [2-9].

There are numerous semi-active control devices such as Magneto-rheological (MR) dampers, Electro-rheological (ER) dampers, variable orifice devices, variable stiffness devices, etc. Among of all the semi-active devices, MR fluid based dampers are the most applicable type due to their valuable characteristics. MR damper includes micron-sized polarizable particles. These particles are dispersed in a carrier medium such as mineral or silicone oil (see Figure 1). MR fluid can change from a linear Newtonian fluid to a nonlinear semi-solid material. This transformation occurs in milliseconds due to change in magnetic field which is imposed on the MR damper. Thus, MR damper properties can change within a very short time when its commanding voltage and magnetic field changes. In addition, MR fluid has a high capacity of energy dissipation, due to the large value of yielding stress [10]. These dampers could be manufactured by a 3D printing technique such as Inject Binder technique which is introduced on Ntintakis et al. [11]. Input voltage of MR damper is the only directly controllable parameter of this damper [12]. Therefore, one of the most important phases of the control process is voltage determination using an appropriate control algorithm.

In some of the semi-active control algorithms such as Clipped Optimal Control (COC), a desired control force is determined using a reference active control algorithm such as LQR, NIOC, H^2/LQG, etc. Consequently, an input voltage is set to achieve this reference active control force via MR damper, [2, 3, 6, 7, 13-15]. In an active-based semi-active control method, the controller is mostly an optimal active controller. The calculated desired active control force is converted to voltage v for current driver and a current i for MR damper. Then, the MR damper produces a control force based on local responses of its installation position and current i. This produced force can be different from the desired control force. Hashemi et al. [16] employed the Bouc-Wen model and developed a wavelet neural network-based semi-active method, which converts the desired control force to the MR damper voltage. Hiramoto et al. [17] proposed a new semi-active control strategy based on a reference active control law. Parameters of the reference active control law were optimized to improve semi-active control performance. Reference active control law predicts desired control forces. Then, based on this predicted control force, the command signal of semi-active control device is determined. The effectiveness of this method is demonstrated through a numerical investigation on a 15-DOF structural system. Liu et al. [18] introduced a semi-active control method using MR damper. They utilized an active-based method for determining the reference control forces via LQR algorithm. This research showed the efficiency of their proposed approach, especially in mitigating the drift and acceleration responses. Zafarani and Halabian [19] developed a model-based semi-active control algorithm for MR dampers. They used a simplified Bouc-Wen model for modelling MR damper hysteretic behavior. They employed active-based semi-active control algorithms for controlling the nonlinear structures. Azar et al. [20] used of three MR dampers through an eleven-story structure. They investigated on optimizing the placement of dampers through the structure. Cruze et al. [21] proposed a new type of MR damper and tested this damper. They used this damper for controlling a scaled structure in a numerical investigation. They concluded this damper is an effective device for alleviating the responses of structure. Jenis et al. [22] proposed a permanent magnet which is installed on MR dampers to promote the abilities of this damper in case of power supply failure.

NIOC method can be used for controlling the nonlinear structures in active control, without the risk of instability of structure [13, 23]. In this algorithm, the control law for the (k+1)'th time step is defined as follows:

$$u_{k+1} = \frac{1}{12}\eta^{-1}R^{*^{-1}}B^{T}\left[Pz_{k+1} + q_{k+1}\right] \quad (1)$$

where B stands for a matrix which locates active control forces vector (u(t)). The NIOC method cost function J is formulated as follows:

$$J_{k+1} = z_{k+1}^{T}Qz_{k+1} + u_{k+1}^{T}Ru_{k+1} \quad (2)$$

Q has to be a positive semi-definite matrix and R must be a positive definite matrix. If Q matrix is chosen relatively large, the response reduction has more importance than the reducing control forces. The NIOC algorithm is used in nonlinear structures as well as linear structures. There is more detailed discussion about the above formulation and notations in Huang et al. [13].

The LQR method uses the subsequent quadratic performance index [6]:

$$J = \int_{\circ}^{\infty} \left[z^T(t) Q z(t) + u^T(t) R u(t) \right] dt \quad (3)$$

The LQR control law is:

$$u = kz \quad (4)$$

k represents the optimal gain matrix which minimizes the performance index J subjected to constraint $\left\{\dot{z}(t) = [A]\{z(t)\} + \{H\}\ddot{x}_g(t) + [B]\{u(t)\}\right\}$. Notations of the LQR method are same as those equations of the NIOC. More discussions are available in Fuller et al. [6] and Pourzeynali et al. [14].

A mathematical representation is mostly required for converting a reference control force to input voltage of MR damper, especially in active-based semi-active control algorithms. Spencer et al. [24] proposed a modified Bouc-Wen model. They investigated on a phenomenological model in comparison with three other mathematical models through a set of experimental tests. They showed that the modified Bouc-Wen model can predict the MR damper behavior more accurately than Bingham, Gamota-Filisko and classic Bouc-Wen models. Cha et al. [12] utilized the modified Bouc-Wen model on their real-time hybrid tests. They identified modelling parameters of the modified Bouc-Wen model of a 200-kN MR damper through some experimental tests. They used this model for controlling a three story office building steel structure by employing active-based semi-active control algorithms. Chae et. al. [10] proposed Maxwell Nonlinear Slider (MNS) model for modelling MR dampers and tested a 300-kN MR damper. This research utilized two other mathematical models for comparison purposes: the modified Bouc-Wen, and the hyperbolic tangent models. Their research showed a good accuracy for the modified Bouc-Wen model. Also, they proved there was a better conformity between the experimental results and the MNS model predictions. Winter and Swartz [25] proposed a small scale MR-fluid extraction damper for testing the small-scale structures equipped with MR dampers. They used a Bouc-Wen model for mathematical representation of the damper. Daniel et al. [4] tested a small scale MR damper within a 3 story small scale structure. They reported that displacement response of all stories was reduced about 50% with a small MR damper which is installed in the 1st story. Rastegarian and Sharifi [26] investigated on the correlation of inter-story drift and performance levels of an RC frame. Here, inter-story drifft is considered as one of assessment criteria. Aghajanzadeh and Mirzabozorg [27] investigated on concrete fracture process which can be undertaken for a RC frame.

In previous researches the main concern of MR damper mathematical model selection was the accuracy and a better agreement between the predictions of the model and the real responses. Effects of mathematical model of MR damper on global control performance of structure are investigated in this research, whereas, no attention was paid earlier. Sapinski et al. [28] and Chae et al. [10] compared different models of MR damper considering the accuracy of modelling with respect to experimental data. Nevertheless, previous researches had not investigated the control performance of these models. Actually, MR damper voltage and resulted control performance of the mentioned models will be different due to differences between the mathematical modeling. As a result, mathematical model selection is an effective part of control of a structure which can effect on control performance and will be investigated here.

At First of all, theoritical background is presented. This section contains an introduction to the MR damper, the modified Bouc-Wen and MNS models, and state-space representation of a system. At the end of this section the applied semi-active control algorithms are described. Next, by the numerical investigations part the utilized reference active control algorithms are designed, and the characteristics of MR dampers and structure which is used for numerical investigations are deployed. In this section, the results of semi-active control of investigated structure are presented. Both the modified Bouc-Wen and MNS models are used in the present research. Finally, conclusions part are summarized.

2. THEORETICAL BACKGROUND

A schematic of a 300-kN MR damper is depicted in Figure 1. This damper, manufactured by Lord Corporation, is used here for numerical investigations. Full characteristics of this large scale MR damper and its identifying tests were deployed by Chae et al. [10]. In subsequent sections, two of the most common models of hysteretic behaviour of an MR damper are introduced, namely: the modified Bouc-Wen, and the MNS models.

2. 1. Modified Bouc-Wen Hysteretic Model A phenomenological Bouc-Wen model is utilized here to model the MR damper. This model is illustrated in Figure 2.

The modified Bouc-Wen model is formulated as follows [12]:

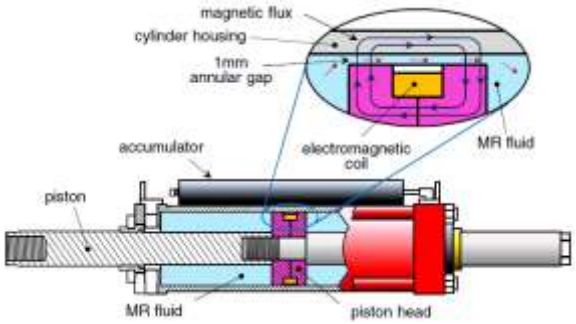

Figure 1. Schematic of the 300-kN MR damper [10]

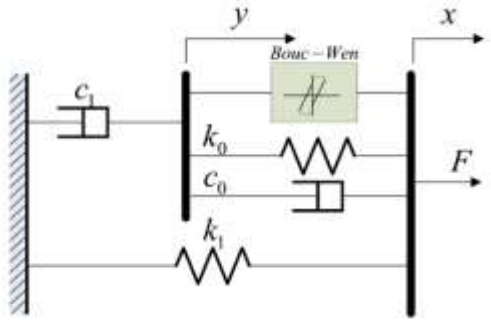

Figure 2. Schematic of mechanical model of MR damper (modified Bouc-Wen model [12, 20])

$$F=\alpha z+c_{\circ}\left(\dot{x}-\dot{y}\right)+k_{\circ}\left(x-y\right)+k_1\left(x-x_{\circ}\right) \quad (5)$$

$$c_1\dot{y}=\alpha z+c_{\circ}\left(\dot{x}-\dot{y}\right)+k_{\circ}\left(x-y\right) \quad (6)$$

$$\dot{z}=-\gamma\left|\dot{x}-\dot{y}\right|z\left|z\right|^{n-1}-\beta\left(\dot{x}-\dot{y}\right)\left|z\right|^{n-1}+A\left(\dot{x}-\dot{y}\right) \quad (7)$$

where F stands for the damper force, c_1 represents the dashpot constant for behavior of MR damper at low velocities, k_1 reveals the accumulator stiffness, c_0 and k_0 denote the damping, and stiffness values at large velocities respectively, x_0 shows the initial displacement of the spring, k_1, α, β, γ, n and A are constants. These parameters have to be identified through experimental tests. The modified Bouc-Wen model was first introduced by Spencer et al. [24], and is utilized in many researches such as Sapinski et al. [28], Cha et al. [12], Chae et al. [10], etc.

2. 2. Maxwell Nonlinear Slider Model A schematic of the MNS model is shown in Figure 3. This model divides the response of an MR damper into two modes: pre-yield and post-yield modes. Pre-yield mode is represented by a Maxwell element, which includes a dashpot with coefficient c and a spring with stiffness k in series. In the pre-yield mode, the damper force f is calculated by solving the following differential equation:

$$f=k\left(y-z\right)=c\dot{z} \quad (8)$$

The responses of the pre-yield mode based on Chae et al. [10] experimental identifying tests are shown in Figure 4. They had compared the MNS and the modified Bouc-Wen models in their paper and they had concluded that the MNS model can predict the response of MR damper more accurate than the modified Bouc-Wen model. These curves were extracted at small amplitudes of harmonic loadings. Post-yield behavior can be divided into separate curves for positive and negative zones (see Figure 5). The following equation is formulated for positive curve of the post-yield mode:

$$f_{py}^{+}\left(\dot{x}\right)=\begin{cases}a^{+}+b^{+}\left|\dot{x}\right|^{n+} & \text{if } \dot{x}\geq\dot{x}_t^{+}\\ a_t^{+}\left(\dot{x}-\dot{x}_t^{+}\right)+f_t^{+} & \text{if } \dot{x}<\dot{x}_t^{+}\end{cases} \quad (9)$$

There is a similar equation for negative curve of the post-yield mode as follows:

$$f_{py}^{-}\left(\dot{x}\right)=\begin{cases}a^{-}+b^{-}\left|\dot{x}\right|^{n-} & \text{if } \dot{x}\leq\dot{x}_t^{-}\\ a_t^{-}\left(\dot{x}-\dot{x}_t^{-}\right)+f_t^{-} & \text{if } \dot{x}>\dot{x}_t^{-}\end{cases} \quad (10)$$

a, b, n and $\dot{x}_t$ are parameters of the MNS model. Also, $a_t^{\pm}=b^{\pm}\times n^{\pm}\times\left|\dot{x}_t^{\pm}\right|^{n^{\pm}-1}$ and $f_t^{\pm}=a^{\pm}+b^{\pm}\left|\dot{x}_t^{\pm}\right|^{n^{\pm}}$.

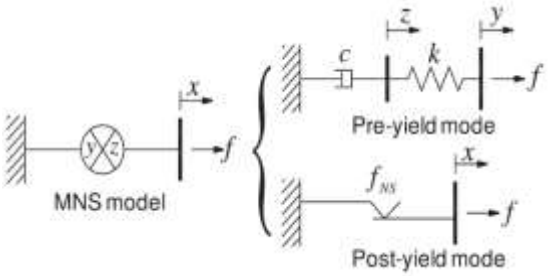

Figure 3. Schematic of mechanical model of MR damper (MNS model [10])

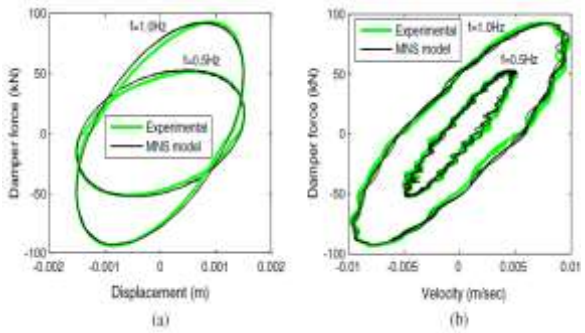

Figure 4. Pre-yield response of MR damper based on the MNS model: a) Force-displacement response. b) Force-velocity response [10]

Based on Figure 6, there is a small difference between increasing and decreasing phases on the MR damper response curves. Taking this issue into account, the subsequent equation is employed:

$$f = \begin{cases} f_{py}(\dot{x}) & \text{increasing phase} \\ f_{py}(\dot{x}) + m_0(\ddot{x}) & \text{decreasing phase} \end{cases} \quad (11)$$

m_0 represents a constant. Chae et al. [10] completely introduced the MNS model at their research.

2. 3. State-Space Representation of Equation of Motion Equation of motion of earthquake-excited structure can be written as follows:

$$[M]\{\ddot{x}\} + [C]\{\dot{x}\} + [K]\{x\} = [M]\{l\}\ddot{x}_g(t) \quad (12)$$

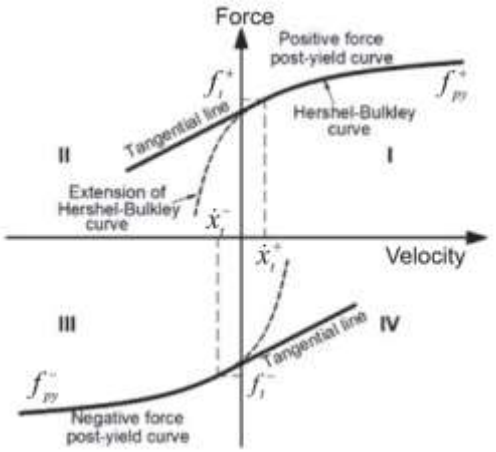

Figure 5. Post-yield curves of the MNS model [10]

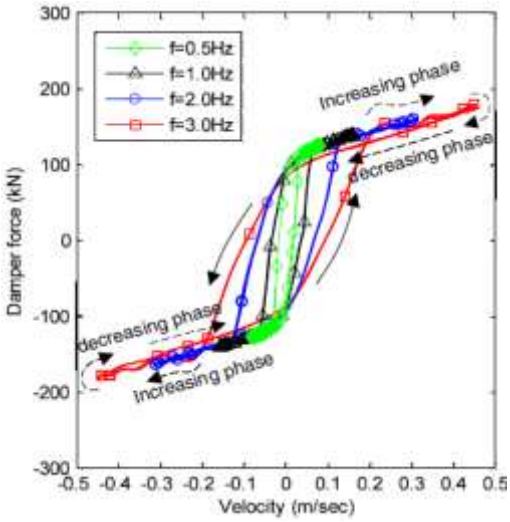

Figure 6. Force-velocity response of MR damper based on the MNS model [10]

[M], [C] and [K] represent the mass, damping, and stiffness matrices, respectively. x , $\dot{x}$ and $\ddot{x}$ denote the relative displacement vector, relative velocity vector, and relative acceleration vector of the system respectively. $\ddot{x}_g$ reveals the ground acceleration. The system can be transferred into state space as follows [6]:

$$\{\dot{z}(t)\} = [A]\{z(t)\} + \{H\}\ddot{x}_g(t) \quad (13)$$

z(t) denotes the state vector of system, [A] represents the open-loop plant matrix and {H} shows a matrix for adjustment of applying point(s) of earthquake inertia force.

$$[A] = \begin{bmatrix} [o] & [I] \\ -[M]^{-1}[K] & -[M]^{-1}[C] \end{bmatrix}_{2n\times 2n} \quad (14)$$

$$\{H\} = \begin{Bmatrix} \{o\} \\ [M]^{-1}\{\delta\} \end{Bmatrix}_{2n\times 1} \quad (15)$$

{δ} adjusts applying point(s) of inertia force, n stands for the number of stories, I and o denote the identity and zero matrices respectively. δ vector is defined as follows:

$$\{\delta\} = [-m_1 \quad -m_2 \quad \ldots \quad -m_n]^T_{n\times 1} \quad (16)$$

Uppercase T suggests the transpose, and m_i represents the seismic mass of the i'th story. There is an introduction to the state space formulation in Fuller et al. [6].

2. 4. Semi-active Control Method Two active-based semi-active control algorithms are employed here: an LQR-based method and an NIOC-based controller. The following steps describe an active-based semi-active control method:

1. An active control law has to be designed first. (Here, the LQR or NIOC)
2. The matrices of structural system are formed at each time step (m, c, and k matrices).
3. Reference active control force is calculated (Using formulation of the introduction part).
4. The reference active control force is converted to voltage of MR damper (Using an iterative procedure).

Based on previous researches such as Chae et al. [10] and Cha et al. [12], the parameters of an MR damper were always identified for some discrete values of currents. Therefore, there are only some discrete values of currents, which can be chosen for a specified mathematical model (e.g. modified Bouc-Wen, MNS, etc.). In the present research, the current determination will be an iterative process during every single time step. In this state, the analysis is implemented for all possible discrete currents, and the best current is selected as the current that commanded the MR damper. It results in better control performance, but at the cost of consuming

more time. The above mentioned procedure is shown on the following flowchart (see Figure 7).

In the subsequent section, a ten-story office building will be used as a prototype steel structure. This structure will be studied for numerical investigation. Two reference active control algorithms are employed to control this structure.: a LQR based, and a NIOC based algorithms. Calculated control force will be converted to input voltage of MR damper. Ten MR dampers will be used for controlling the prototype ten-story structure.

3. NUMERICAL INVESTIGATIONS

A ten story office building steel structure is employed here for numerical investigations where all stories have an equal area of 22500 square feet. There are 6 bays in each direction with 25-ft width, and the height of all stories is 12.5-ft. Each primary direction is composed of eight MRF and four DBF in each primary direction. In Figure 8, MRF's are shown in blue color and DBF's depicted in yellow color, respectively. Plan of the structure is shown in Figure 7. The plan of this structure is very similar to Cha et al. [12]. In this office building, considerations and preservations of Pinheiro [29] and Burciaga [30] could be undertaken to make a green building.

This structures have a full symmetry in both primary directions of plan. In all four corners of plan, two columns are designed to maintain the full independence of two primary directions (see Figure 8). Therefore, only one-fourth of total area would be analyzed as tributary seismic area. Also, two directions will be considered independently due to symmetry principles. Cha et al. [12] used 0.6-scale model of three-story structure as shown in Figure 9a. Here, the full-scale structure is employed (see Figure 9b).

All diaphragms are supposed to be rigid. Now, two MRF of the structure will be analyzed in order to execute numerical investigations. Vertical degrees of freedom are eliminated using the static condensation method. Therefore, mass, and stiffness matrices of structure are extracted through finite element method. The damping matrix is calculated using the Rayleigh method with five percent of critical damping for the first, and the second mode of vibration.

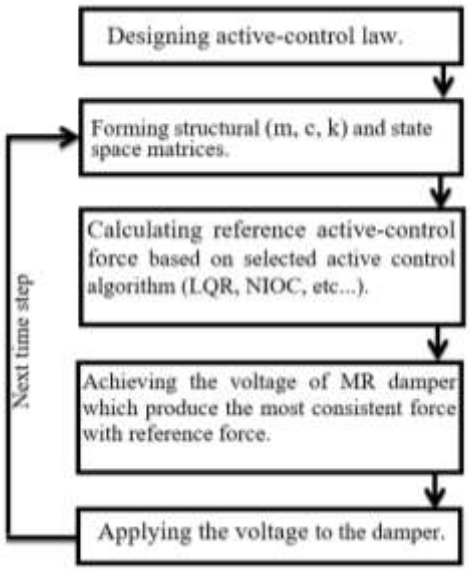

Figure 7. A schematic of the employed semi-active control algotithm

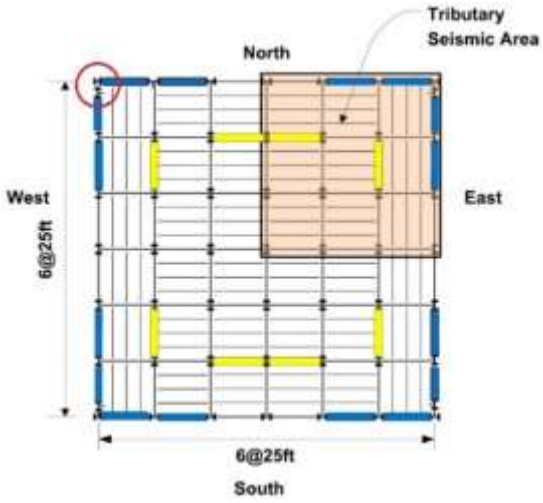

Figure 8. Structure model

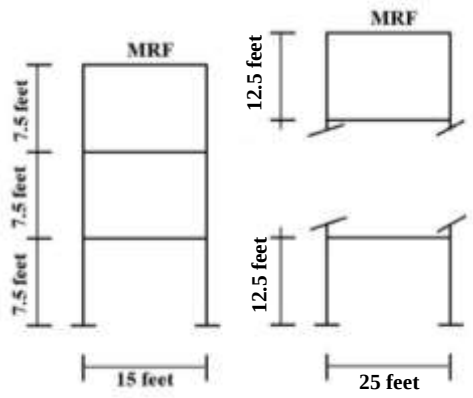

a.Three-story structure (Cha et al. [12]) b. Ten-story structure (Present study)

Figure 9. MRF frame model

The mass, damping, and initial stiffness matrices of structures are presented as follows:

[m]=

330000	0	0	0	0
0	326000	0	0	0
0	0	323000	0	0
0	0	0	322000	0
0	0	0	0	320000
0	0	0	0	0
0	0	0	0	0
0	0	0	0	0
0	0	0	0	0
0	0	0	0	0
0	0	0	0	0
0	0	0	0	0
0	0	0	0	0
0	0	0	0	0
0	0	0	0	0
319000	0	0	0	0
0	318000	0	0	0
0	0	316000	0	0
0	0	0	313000	0
0	0	0	0	301000

[C] =

1.15E+07	-5246889	971737.6	-165530	40224.73
-5246891	6520370	-3413867	673343.8	-78075
971737.9	-3413867	4945671	-2787034	506984.9
-165530	673343.5	-2787035	4282808	-2413674
40224.44	-78075.3	506984.6	-2413674	3682740
-8833.97	25294.38	-60835.9	438292	-2023057
1574.682	-5093.4	15474.84	-43469.3	372554.2
399.4307	1389.553	-2183.21	11366.06	-33629.4
-216.537	-175.655	44.15915	-2047.97	6975.204
932.3492	942.9214	1941.575	1528.17	-1051.23
-8833.88	1574.8	399.9862	-216.754	933.1585
25294.48	-5093.28	1390.091	-175.864	943.7005
-60835.8	15474.94	-2182.69	43.95329	1942.332
438292.1	-43469.1	11366.6	-2048.17	1528.935
-2023057	372554.3	-33628.9	6974.999	-1050.49
3160785	-1772419	299773.9	-16448.1	4307.57
-1772420	2722533	-1411131	180816.5	-11936.3
299773.6	-1411132	1935697	-875542	121494.1
-16447.9	180816.6	-875542	1364456	-609938
4306.851	-11937	121493.5	-609939	536925.5

[k] =

8.95E+08	-4.10E+08	7.60E+07	-1.29E+07	3.15E+06
-4.10E+08	5.06E+08	-2.67E+08	5.27E+07	-6.11E+06
7.60E+07	-2.67E+08	3.83E+08	-2.18E+08	3.96E+07
-1.29E+07	5.27E+07	-2.18E+08	3.31E+08	-1.89E+08
3.15E+06	-6.11E+06	3.96E+07	-1.89E+08	2.84E+08
-6.91E+05	1.98E+06	-4.76E+06	3.43E+07	-1.58E+08
1.23E+05	-3.98E+05	1.21E+06	-3.40E+06	2.91E+07
3.12E+04	1.09E+05	-1.71E+05	8.89E+05	-2.63E+06
-1.69E+04	-1.37E+04	3.45E+03	-1.60E+05	5.46E+05
7.29E+04	7.37E+04	1.52E+05	1.20E+05	-8.22E+04
-6.91E+05	1.23E+05	3.13E+04	-1.70E+04	7.30E+04
1.98E+06	-3.98E+05	1.09E+05	-1.38E+04	7.38E+04
-4.76E+06	1.21E+06	-1.71E+05	3.44E+03	1.52E+05
3.43E+07	-3.40E+06	8.89E+05	-1.60E+05	1.20E+05
-1.58E+08	2.91E+07	-2.63E+06	5.45E+05	-8.22E+04
2.43E+08	-1.39E+08	2.34E+07	-1.29E+06	3.37E+05
-1.39E+08	2.09E+08	-1.10E+08	1.41E+07	-9.33E+05
2.34E+07	-1.10E+08	1.48E+08	-6.85E+07	9.50E+06
-1.29E+06	1.41E+07	-6.85E+07	1.03E+08	-4.77E+07
3.37E+05	-9.34E+05	9.50E+06	-4.77E+07	3.84E+07

All matrices are presented in S.I. units. One can calculate the period of vibration modes utilizing an eigen analysis using the [k] and [m] matrices. It leads to 3.02, 1.09 and 0.62 s for the first three modes of vibration respectively. On the other hand, the analysis results of 3d model in the OpenSees™ finite element software show these periods as 3.05, 1.09 and 0.61 s respectively. These are very coincident.

Seven acceleration time histories are used here. Each record has a different value of PGA. Four records are scaled based on ASCE/SEI7-10 [31] method and three records are originally used as unscaled records. NORT, Kobe, Elcent and IMP records are scaled records. These are listed in the following Table 1. Large values of PGA, make the structure behave nonlinearly during analysis. Also, response spectrum of seven acceleration time histories are shown in Figure 10.

300-kN MR dampers are used here for numerical investigations. One MR damper will be installed in each single story. Therefore, there will be ten MR dampers for the ten-story structure. Parameters of these dampers were identified in Chae et al. [10] during experimental tests and used in the present paper. These parameters were given for discrete values of currents: 0, 0.5, 1.0, 1.5, 2.0 and 2.5 A.

Q and R matrices of LQR-based, and NIOC-based semi-active control methods are considered as Equation (17) and Equation (18).

$$Q = \rho \times \begin{bmatrix} 1 & \cdots & \circ \\ \vdots & \ddots & \vdots \\ \circ & \cdots & 1 \end{bmatrix}_{2n \times 2n} \tag{17}$$

TABLE 1. Acceleration time histories

Record Name	Earthquake	Year	Station Name	PGA
SAN	San Fernando	1971	Old Ridge Root	0.32g
Elcent	Elcentro	1940	Elcentro Array 9	0.50g
NORT	Northridge	1994	Alhambra 90	0.50g
VICT	Victoria Mexico	1980	Cerro Prieto	0.63g
Tabas	Tabas	1978	Tabas	0.86g
Kobe	Kobe	1995	Kobe University	1.00g
IMP	Imperial Valley	1979	Elcentro Array	1.50g

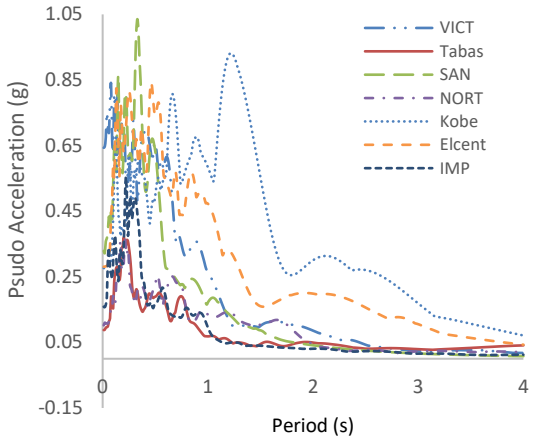

Figure 10. Response spectrum of the used acceleration time histories

$$R=\begin{bmatrix}1 & \cdots & \circ\\ \vdots & \ddots & \vdots\\ \circ & \cdots & 1\end{bmatrix}_{n\times n} \quad (18)$$

Coefficient of Q weighting matrix (ρ) is adjusted based on a set of pre-analysis results. When Q is selected relatively large, reducing the responses has more importance than reducing the control forces, and vice versa. Here, the allowable values for the maximum of control forces is set to 10% of the structural total seismic weight. On the contrary, if Q matrix is selected relatively small, then, the control performance would not be acceptable. Therefore, an optimum value has to be chosen. Two levels of control are introduced: cheap control and expensive control. In the cheap mode of control, small value of the maximum of control forces will be achieved, and the expensive mode of control tries to achieve the best control performance with a larger value of maximum of control forces. The ρ coefficient is adjusted for different control algorithms and different control modes based on previous comments. The results are listed in Table 2.

Three comparative criteria are introduced. The first is drift criterion, the second criterion belongs to residual drift, and the third one denotes hysteretic energy.

$$J_1=\left\{\frac{\max_{t,i}|\Delta_i(t)|}{\max_{t,i}|\Delta_{iU}(t)|}\right\} \quad (19)$$

$\Delta_i(t)$ represents the interstory drift of *i*'th story at time t and $\Delta_{iU}(t)$ shows the interstory drift of the uncontrolled structure at time t. J_2 criterion is defined as follows:

$$J_2=\left\{\frac{\max_i|\Delta_{iR}|}{\max_i|\Delta_{iRU}|}\right\} \quad (20)$$

TABLE 2. Coefficient of Q weighting matrix (ρ).

ρ Coefficient	cheap control	expensive control
LQR	1.0 e +11	3.0 e +11
NIOC	6.0 e +13	1.5 e +14

Δ_{iR} represents the residual drift of *i*'th story at the end of analysis, and Δ_{iRU} shows the residual drift of *i*'th story of the uncontrolled structure at the end of analysis.

$$J_3=\left\{\frac{\max_i E_{hi}}{\max_i E_{hUi}}\right\} \quad (21)$$

E_{hi} represents the total hysteretic energy of *i*'th story and E_{hUi} stands for the total hysteretic energy of i'th story of the uncontrolled structure. It should be noted that the hysteretic energy is calculated for moment-rotation curve of both ends of each beam.

UI Sim-Cor™ is implemented for analyzing the structure. This hybrid simulation code employs the OpenSees™, and Matlab™ softwares simultaneously. Implicit Newmark integration method with alpha equal to 0.25 and beta equal to 0.1667 is used. Results of analysis based on prementioned notes are calculated and listed in Table 3. In this table, the average values of the modified Bouc-Wen model and the MNS model are calculated for each mode of control. The ratio of average values of these two mathematical models are calculated in the Bouc/MNS rows. In addition to three defined criteria, the maximum of control forces among all stories are listed in the table.

TABLE 3. Results of evaluation criteria for ten-story structure

	LQR Based		NIOC Based	
	Cheap	Expensive	Cheap	Expensive
J1				
SAN Bouc	0.971	0.904	0.976	0.876
SAN MNS	0.952	0.828	0.957	0.761
Elcent Bouc	0.967	0.793	0.894	0.826
Elcent MNS	0.968	0.773	0.869	0.833
NORT Bouc	1.011	0.948	0.856	0.908
NORT MNS	1.009	0.945	0.848	0.896
VICT Bouc	0.954	0.849	0.911	0.737
VICT MNS	0.947	0.829	0.891	0.707
Tabas Bouc	0.881	0.739	0.883	0.823
Tabas MNS	0.875	0.732	0.88	0.82
Kobe Bouc	0.973	1.008	0.979	0.979
Kobe MNS	0.973	1.015	0.974	0.982
IMP Bouc	0.956	0.845	0.883	0.762
IMP MNS	0.945	0.848	0.85	0.768

Average Bouc	0.959	0.869	0.912	0.844
Average MNS	0.953	0.853	0.896	0.824
Bouc/MNS	1.007	1.019	1.018	1.025
J2				
SAN Bouc	0	0	0	0
SAN MNS	0	0	0	0
Elcent Bouc	0.8215	0.5531	0.8582	0.7140
Elcent MNS	0.8113	0.5334	0.7998	0.7183
NORT Bouc	0.9335	1.1168	0.9687	1.6330
NORT MNS	1.0008	1.1254	0.9090	1.6561
VICT Bouc	0	0	0	0
VICT MNS	0	0	0	0
Tabas Bouc	0.9640	0.9036	0.7460	0.5495
Tabas MNS	0.9837	0.8464	0.7371	0.5210
Kobe Bouc	1.0204	1.1593	1.0360	1.0688
Kobe MNS	1.0248	1.1721	1.0277	1.0937
IMP Bouc	0.9148	0.9069	1.0109	0.8535
IMP MNS	0.8912	0.9298	0.9678	0.9336
Average Bouc	0.6649	0.6628	0.6600	0.6884
Average MNS	0.6731	0.6581	0.6345	0.7032
Bouc/MNS	0.9878	1.0071	1.0401	0.9789
J3 (HE)				
SAN Bouc	0.961	0.955	0.988	0.928
SAN MNS	0.935	0.899	0.935	0.858
Elcent Bouc	0.801	0.566	0.904	0.711
Elcent MNS	0.772	0.558	0.902	0.706
NORT Bouc	0.773	0.524	0.564	0.424
NORT MNS	0.776	0.509	0.545	0.4
VICT Bouc	0.948	0.902	1.094	0.947
VICT MNS	0.929	0.885	0.945	0.854
Tabas Bouc	0.771	0.545	0.764	0.606
Tabas MNS	0.765	0.537	0.766	0.6
Kobe Bouc	0.909	0.851	0.942	0.874
Kobe MNS	0.904	0.85	0.938	0.871
IMP Bouc	0.73	0.459	0.778	0.579
IMP MNS	0.713	0.459	0.835	0.54
Average Bouc	0.842	0.686	0.862	0.724
Average MNS	0.828	0.671	0.838	0.69
Bouc/MNS	1.017	1.022	1.028	1.05
Control Force				
SAN Bouc	31	84	30	128
SAN MNS	44	84	84	131
Elcent Bouc	155	246	145	254
Elcent MNS	157	242	137	246
NORT Bouc	129	240	239	236
NORT MNS	122	238	237	235
VICT Bouc	49	92	96	135
VICT MNS	46	93	97	138
Tabas Bouc	142	232	266	264
Tabas MNS	145	232	252	250
Kobe Bouc	310	310	244	308
Kobe MNS	274	273	229	272
IMP Bouc	169	276	187	274
IMP MNS	168	261	180	259
Average Bouc	141	211	173	228
Average MNS	136	203	174	219
Bouc/MNS	1.03	1.04	0.99	1.04

Figures 11 to 15 illustrate some of analysis results. Figures 11 and 12 show average of drifts and average of residual drifts through the height of structure, respectively. Figures 13 and 14 display force-displacement and force-velocity response of MR damper where attached to the 3rd story, respectively. Finally, Figure 15 illustrates time history of maximum of drifts under Elcentro record. These figures prove that there are differences between the modified Bouc-Wen model and the MNS model in control performance of an MR damper. It means, using each mathematical MR damper model can lead to different control forces.

Based on Figure 11 to Figure 15 and Table 3, some notes on control algorithms and mathematical modelling methods are remarkable:

a. The MNS model performs better than the modified Bouc-Wen model in J_3 criterion. In other words, the MNS model has outperformed the other model in reducing the maximum of hysteretic energy. This observation is correct for the averages of all the control algorithms, and all the control modes.
b. There is no pronounced difference between these two models in reducing the drift response, and residual drift.
c. The NIOC-based semi-active control algorithm has outperformed the LQR-based algorithm in reducing the drift response for all modes of control.
d. The LQR-based control algorithm has outperformed the NIOC-based algorithm in reducing the maximum of hysteretic energy for all modes of control.
e. The NIOC-based control algorithm has reduced the residual drift more than the LQR-based algorithm for the cheap mode of control.

f. The LQR-based control algorithm has reduced the residual drift more than the NIOC-based algorithm for the expensive mode of control.
g. The maximum of control forces of these two algorithms for the expensive mode of control is the same.
h. The maximum of required control forces for the MNS model is slightly less than modified Bouc-Wen model.
i. The MNS model requires a smaller capacity of MR damper for all modes of control, while it performs better than the modified Bouc-Wen model especially in J_1, and J_3 criteria. In other words, the MNS model would be an appropriate choice when reducing the drift and hysteretic energy are considered.
j. Choosing the LQR-based algorithm for all modes of control leads to a smaller capacity of MR damper.
k. Figures 11, 12, and 15 display the effectiveness of all control modes and algorithms in controlling the structure in comparison with uncontrolled structure. This advantage occurs in drift and residual drift.

There is another point; Figure 12 shows a more uniformity in residual drifts for controlled structure. This concept may lead to damage reduction in a structure. Residual drift and hysteretic energy are distributed more uniform through the entire structure. As a result, the MNS model has a higher performance than the modified Bouc-Wen model. Using the MNS model the acceleration responses and the maximum of hysteretic energy of the ten-story structure is more reduced with smaller control forces. Therefore, as the MNS model is a more accurate model, it has outperformed the modified Bouc-Wen model from the control performance point of view.

It should be noted that there is no considerable difference between the two investigated models in time cost of analysis.

4. SUMMARY AND CONCLUSION

A comparative study on two mathematical models of MR damper has been implemented in this research: the modified Bouc-Wen model and the MNS model. These models are employed in this research through two active-based semi-active control algorithms on a nonlinear ten story office building structure: an LQR based and a NIOC based semi-active control algorithms. Ten 300-kN MR dampers utilized, are each installed on a single story. analysis. For better contrast, two control modes are set: the cheap mode of control with smaller Q weighting matrix and the expensive mode of control with larger values of Q matrix.

The drift of the 3rd floor and the 9th floor of the ten-story structure is more than other stories, based on Figure 11. On the other side, the residual drift of the 9th floor is larger, based on Figure 12. As a result, control of the 9th floor responses is more important than other floors. The MNS model has reduced the maximum drift and the residual drift of the 9th floor better than the modified Bouc-Wen model based on Figures 11 and 12 for both control algorithms. Therefore, the MNS model can control the maximum damage of structure, more than the modified Bouc-Wen model, if damage index is supposed as a combination of maximum drift and residual drift of each story.

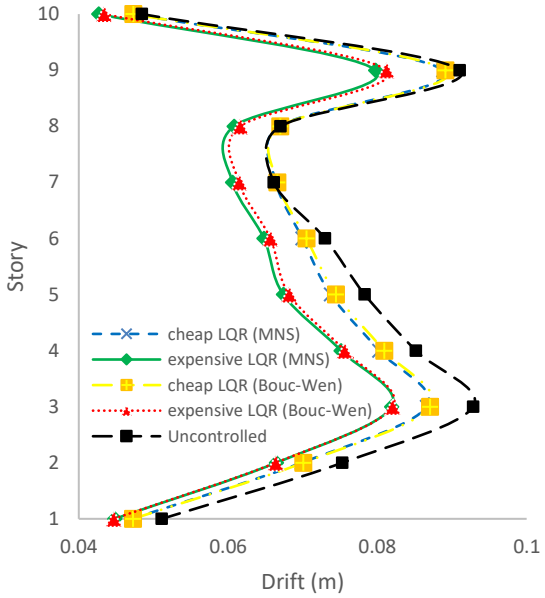

(a) LQR method vs. uncontrolled

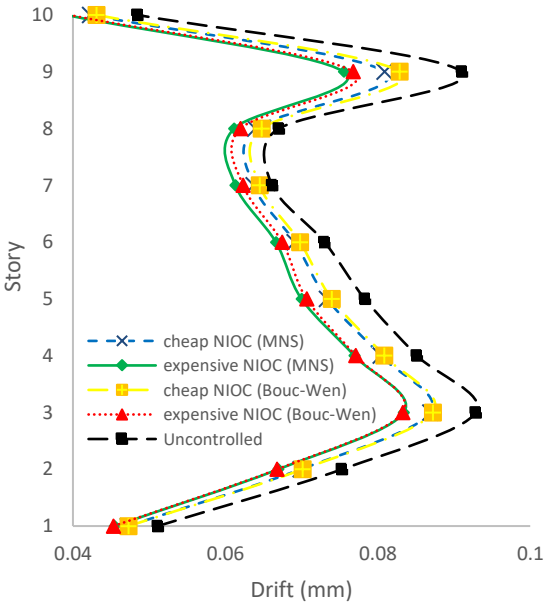

(b) NIOC method vs. uncontrolled

Figure 11. Diagram of the average of maximum story drifts

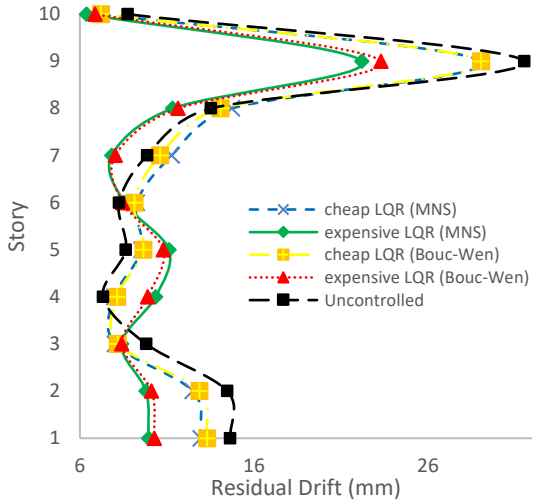

(a) LQR method vs. uncontrolled

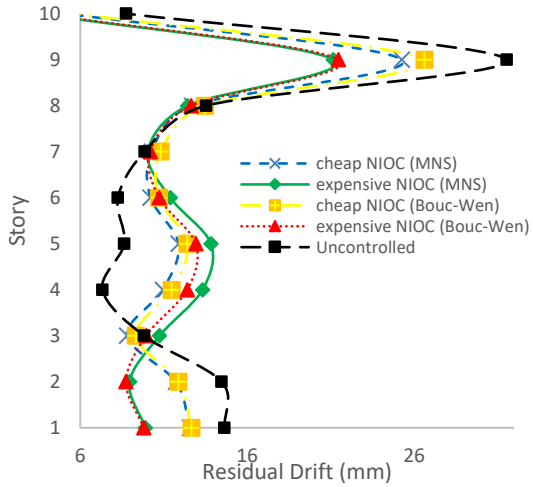

(b) NIOC method vs. uncontrolled

Figure 12. Diagram of the average of residual drifts for Elcentro, Tabas and IMP records

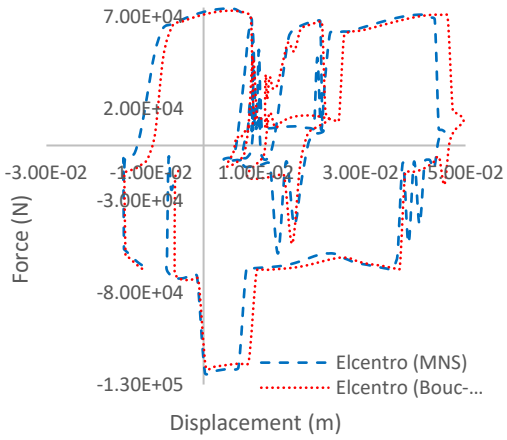

The 3rd story

Figure 13. Diagram of the force–displacement of the MR damper of the 3rd floor (control algorithm: LQR-based semi-active)

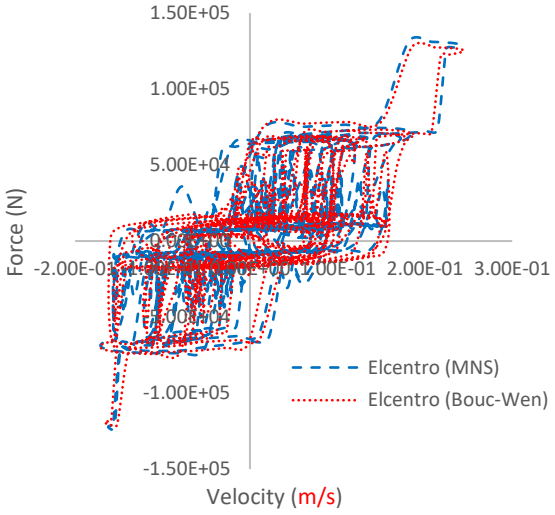

The 3rd story

Figure 14. Diagram of the force – velocity of the MR damper of the 3rd floor (control algorithm: LQR-based semi-active)

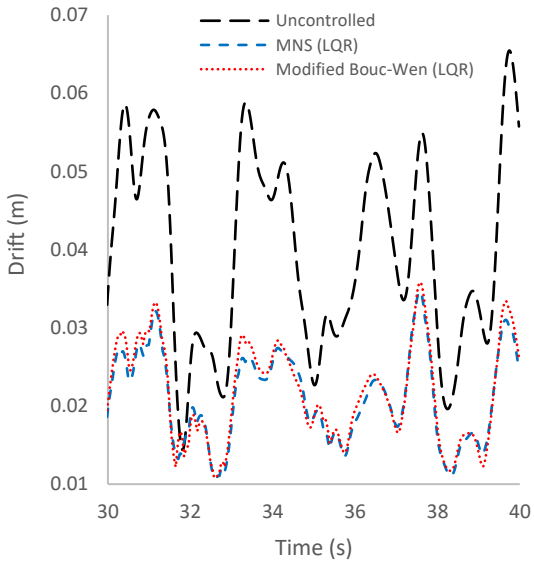

Figure 15. Time history of the maximum of drifts (expensive mode of control of the Elcentro record)

Final results show a slight superiority for the MNS model in reducing the hysteretic energy, and maximum of drifts while this model requires smaller capacity of MR dampers in comparison with the modified Bouc-Wen model. This point can be used for mathematical model selection in a control practic. Based on Cha et al. [12], the MNS model has also more accuracy. Then, the MNS hysteretic model looks more appropriate for using in semi-active control via MR dampers, especially in mid-rise building structures.

The LQR-based algorithm, results in a higher control performance for reducing the maximum of hysteretic energy, and residual drifts. Also, the NIOC-based algorithm requires a larger capacity of MR dampers. Nevertheless, it reduces the maximum of drifts responses more than the LQR-based algorithm. Finally, it can be extracted that the NIOC-based control algorithm containing the MNS hysteretic model is more prefered for control of building structures via MR dampers.

Time delay and measurement noise probable effects on the control performance of two investigated algorithms should be studied. Also, more researches are required for evaluating the impacts of structural height on the results and conclusions. Other mathematical hysteretic models of MR damper such as standard Bouc-Wen model, bilinear model etc. can be used for a better outcome.

5. REFERENCES

1. Ha, Kwangtae, "Innovative Blade Trailing Edge Flap Design Concept Using Flexible Torsion Bar and Worm Drive", ***HighTech and Innovation Journal,*** Vol. 1, No. 3, (2020). https://dx.doi.org/10.28991/HIJ-2020-01-03-01.
2. Cheng, Y. F., Jiang, H., Lou, K., SMART STRUCTURES, Innovative systems for Seismic Response Control, CRC Press, 2008. doi:https://doi.org/10.1201/9781420008173
3. Connor, J. J., Introduction to Structural Motion Control. Pearson Education Ltd., 2003. doi:978-3-319-06281-5
4. Daniel, C., Hemalatha, G., Sarala, L., Tensing, D., & Sundar Manoharan, S., "Seismic Mitigation of Building Frames using Magnetorheological Damper", ***International Journal of Engineering Transactions A: Basics,*** (2019), 1543-1547. doi:10.5829/ije.2019.32.11b.05
5. Dyke, S. J., Spencer Jr., B. F., Sain, M. K., Carlson, J. D., "Experimental Verification of Semi-Active Structural Control Strategies Using Acceleration Feedback", Proceedings of the 3rd International Conference on Motion and Vibration Control, (1996), 291-296, Chiba, Japan.
6. Fuller, C. R., Elliott, S. J., Nelson, P. A., Active Control of Vibration. Academic Press, 1996.
7. Jansen, L. M., Dyke, S. J., "Semi-Active Control Strategies for MR Dampers: A Comparative Study", ***Journal of Engineering Mechanics***, (2000), 795-803. doi:10.1061/(ASCE)0733-9399(2000)126:8(795)
8. Soong, T. T., Active Structural Control: Theory and Practice. NY: Longman Group. Retrieved from, 1990. https://doi.org/10.1061/(ASCE)0733-9399(1992)118:6(1282)
9. Soong, T. T., Dargush, G. F., Passive Energy Dissipation Systems in Structural Engineering. John Wiley & Sons, Ltd. (UK), 1997.
10. Chae, Y., Ricles, J. M., Sause, R., "Modeling of a large-scale magneto-rheological damper for seismic hazard mitigation. Part I: Passive mode", ***Earthquake Engineering & Structural Dynamics,*** Vol. 42, (2013), 669-685. doi:10.1002/eqe.2237
11. Ntintakis, I., Stavroulakis, G., E., Plakia, N., "Topology Optimization by the Use of 3D Printing Technology in the Product Design Process", ***HighTech and Innovation Journal***, Vol. 1, No. 4, (2020). https://dx.doi.org/10.28991/HIJ-2020-01-04-03.
12. Cha, Y.J., Zhang, J., Agrawal, A. K., Dong, B., Friedman, A., Dyke, S. J., Ricles, J., "Comparative Studies of Semiactive Control Strategies for MR Dampers: Pure Simulation and Real-Time Hybrid Tests", ***Journal of Structural Engineering,*** (2013), 1237-1248. doi:10.1061/(ASCE)ST.1943-541X.0000639
13. Huang, K., Betti, R., Ettouney, M. M., "Instantaneous Optimal Control for Seismic Analysis of Non-Linear Structures", ***Journal of Earthquake Engineering,*** Vol. 3, No. 1, (1999), 83-106. doi:10.1002/eqe.322
14. Pourzeynali, S., Jooei, P., "Semi-active Control of Building Structures using Variable Stiffness Device and Fuzzy Logic", ***International Journal of Engineering, Transactions A: Basics***, (2013), 1169-1182. doi:10.5829/idosi.ije.2013.26.10a.07
15. Pourzeynali, S., Malekzadeh, M., Esmaeilian, F., "Multi-objective Optimization of Semi-active Control of Seismically Exited Buildings Using Variable Damper and Genetic Algorithms", ***International Journal of Engineering Transactions A: Basics,*** (2012), 265-276. doi:10.5829/idosi.ije.2012.25.03a.08
16. Hashemi, S., Haji Kazemi, H., Karamodin, A., "Localized genetically optimized wavelet neural network for semiactive control of buildings subjected to earthquake", ***Structural Control and Health Monitoring***, (2016). doi:10.1002/stc.1823
17. Hiramoto, K., Matsuoka, T., Sunakoda, K., "Semi-active vibration control of structural systems based on a reference active control law: output emulation approach", ***Structural Control and Health Monitoring***, Vol. 23, (2016), 423-445. doi:10.1002/stc.1770
18. Liu, Y.-F., Lin, T.-K., Chang, K.-C., "Analytical and experimental studies on building mass damper system with semi-active control device", ***Structural Control and Health Monitoring***, (2018). doi:https://doi.org/10.1023/A:1004442832316
19. Zafarani, M., Halabian, A., "Supervisory adaptive nonlinear control for seismic alleviation of inelastic asymmetric buildings equipped with MR dampers", ***Engineering Structures,*** Vol. 176, (2018), 849-858. doi:10.1016/j.engstruct.2018.09.045
20. Azar, B. F., Veladi, H., Talatahari, S., Raeesi, F., "Optimal design of magnetorheological damper based on tuning Bouc-Wen model parameters using hybrid algorithms", ***KSCE Journal of Civil Engineering***, (2020), 867-878. doi:10.1007/s12205-020-0988-z
21. Cruze, D., Gladston, H., Farsangi, E., Loganathan, S., Dharmaraj, T., Solomon, S., "Development of a Multiple Coil Magneto-Rheological Smart Damper to Improve the Seismic Resilience of Building Structures", ***The Open Civil Engineering Journal,*** (2020). doi:10.2174/1874149502014010078
22. Jeniš, F., Kubík, M., Macháček, O., Šebesta, K., Strecker, Z.,"Insight into the response time of fail-safe magnetorheological damper", ***Smart Materials and Structures,*** (2020).
23. Yang, J. N., Long, F. X., Wong, D., "Optimal Control of Nonlinear Structures", ***Journal of Applied Mechanics,*** (1988), 931-938. doi:https://doi.org/10.1115/1.3173744
24. Spencer Jr., B. F., Dyke, S. J., Sain, M. K., Carlson, J. D., "Phenomenological Model For Magnetorheological Dampers", ***Journal of Engineering Mechanics,*** (1997), 230-238. doi:10.1061/(ASCE)0733-9399(1997)123:3(230)
25. Winter, B. D., Swartz, R. A., "Low-force magneto-rheological damper design for small-scale structural control", ***Structural Control and Health Monitoring,*** (2017). https://doi.org/10.1016/j.tafmec.2019.03.0122
26. Rastegarian, S., Sharifi, A., "An Investigation on the Correlation of Inter-Story drift and Performance Objectives in Conventional RC Frames", ***Emerging Science Journal***, Vol. 2, No. 3, (2018). https://dx.doi.org/10.28991/esj-2018-01137.

27. Aghajanzadeh, S.M. Mirzabozorg, H., "Concrete Fracture Process Modeling by Combination of Extended Finite Element Method and Smeared Crack Approach", ***Theoritical and Applied Fracture Mechanics***, (2019).
28. Sapinski, B., Filus, J., "Analysis of Parametric Models of MR Linear Damper", ***Journal of Theoretical and Applied Mechanics***, Vol. 41, No. 2, (2002), 215-240. doi: 10.1.1.453.2815
29. Pinheiro, Ana Paula, "Architucturral Rehabilitation and Sustainability of Green Buildings in Historic Preservation", ***HighTech and Innovation Journal,*** Vol. 1, No. 4, (2020). https://dx.doi.org/10.28991/HIJ-2020-01-04-04.
30. Burciaga, Ulises Mercado, "Sustainability Assessment in Housing Building Organizations for the Design of Strategies against Climate Change", ***HighTech and Innovation Journal,*** Vol. 1, No. 4, (2020). https://dx.doi.org/10.28991/HIJ-2020-01-04-01.
30. American Society of Civil Engineers, & Structural Engineering Institute, "Minimum Design Loads for Buildings and Other Structures", *ASCE/SEI*., 2010.

Persian Abstract

چکیده

موضوع مقاله حاضر مقایسه دو روش مختلف مدل‌سازی رفتار چرخه‌ای میراگر نیمه‌فعال MR می‌باشد. این مقایسه با تاکید بر تاثیر این مدل‌ها بر کیفیت اثر کنترلی میراگر بر سازه‌های غیرخطی صورت پذیرفته است. در مقاله حاضر از دو مدل بوک- ون اصلاح شده و لغزنده غیرخطی ماکسول به جهت مدل‌سازی رفتار چرخه‌ای میراگر استفاده شده است. نیز دو الگوریتم کنترلی شناخته‌شده‌ی LQR و NIOC به جهت تعیین نیروهای کنترلی مورد استفاده قرار گرفته‌اند. در بخشی از روند تعیین نیروهای کنترلی میراگر MR ، استفاده از روش مدل‌سازی رفتار چرخه‌ای میراگر ضروری می‌باشد. بر این اساس مقایسه ای بین میزان کاهش برخی پاسخ‌های سازه مانند جابه‌جایی نسبی بین طبقات، انرژی چرخه‌ای تیرهای طبقات و جابه‌جایی مانده در طبقات با بهره‌گیری از هر کدام از روش‌های مدل‌سازی ذکرشده صورت پذیرفته است. یک سازه ده طبقه اسکلت فلزی با کاربری اداری به جهت بررسی موضوع مقاله حاضر مورد بررسی قرار گرفته است. تحلیل‌های تاریخچه زمانی غیرخطی بر روی این سازه با استفاده از هفت شتاب نگاشت زلزله با بزرگا و خصوصیات مختلف انجام شده است. نتایج تحلیل‌ها، نشان از تفاوت نسبی پاسخ‌های سازه در استفاده از هر یک از دو روش مدل‌سازی یادشده دارد.